Hydrol. Earth Syst. Sci., 21, 533–548, 2017
www.hydrol-earth-syst-sci.net/21/533/2017/
doi:10.5194/hess-21-533-2017

Hydrology and Earth System Sciences
Open Access
EGU

Response of water vapour D-excess to land–atmosphere interactions in a semi-arid environment

Stephen D. Parkes[1], Matthew F. McCabe[1,2], Alan D. Griffiths[3], Lixin Wang[4], Scott Chambers[3], Ali Ershadi[1,2], Alastair G. Williams[3], Josiah Strauss[2], and Adrian Element[3]

[1]Water Desalination and Reuse Centre, King Abdullah University of Science and Technology (KAUST), Jeddah, Saudi Arabia
[2]Department of Civil and Environmental Engineering, University of New South Wales, Sydney, Australia
[3]Australian Nuclear Science and Technology Organization, Sydney, New South Wales, Australia
[4]Department of Earth Sciences, Indiana University – Purdue University Indianapolis (IUPUI), Indianapolis, IN, USA

Correspondence to: Stephen D. Parkes (stephen.parkes@kaust.edu.sa)

Received: 2 June 2016 – Published in Hydrol. Earth Syst. Sci. Discuss.: 30 June 2016
Revised: 15 December 2016 – Accepted: 18 December 2016 – Published: 27 January 2017

Abstract. The stable isotopic composition of water vapour provides information about moisture sources and processes difficult to obtain with traditional measurement techniques. Recently, it has been proposed that the D-excess of water vapour ($d_v = \delta^2H - 8 \times \delta^{18}O$) can provide a diagnostic tracer of continental moisture recycling. However, D-excess exhibits a diurnal cycle that has been observed across a variety of ecosystems and may be influenced by a range of processes beyond regional-scale moisture recycling, including local evaporation (ET) fluxes. There is a lack of measurements of D-excess in evaporation (ET) fluxes, which has made it difficult to assess how ET fluxes modify the D-excess in water vapour (d_v). With this in mind, we employed a chamber-based approach to directly measure D-excess in ET (d_{ET}) fluxes. We show that ET fluxes imposed a negative forcing on the ambient vapour and could not explain the higher daytime d_v values. The low d_{ET} observed here was sourced from a soil water pool that had undergone an extended drying period, leading to low D-excess in the soil moisture pool. A strong correlation between daytime d_v and locally measured relative humidity was consistent with an oceanic moisture source, suggesting that remote hydrological processes were the major contributor to daytime d_v variability. During the early evening, ET fluxes into a shallow nocturnal inversion layer caused a lowering of d_v values near the surface. In addition, transient mixing of vapour with a higher D-excess from above the nocturnal inversion modified these values, causing large variability during the night. These results indicate d_{ET} can generally be expected to show large spatial and temporal variability and to depend on the soil moisture state. For long periods between rain events, common in semi-arid environments, ET would be expected to impose negative forcing on the surface d_v. Spatial and temporal variability of D-excess in ET fluxes therefore needs to be considered when using d_v to study moisture recycling and during extended dry periods with weak moisture recycling may act as a tracer of the relative humidity at the oceanic moisture source.

1 Introduction

Climate change has the potential to significantly impact surface and atmospheric water budgets. Our best understanding of future exchanges between the atmospheric water cycle and the land surface for regional to global scales is likely to be gained through analysis of numerical simulations (Decker et al., 2015; Evans and McCabe, 2010; Harding and Snyder, 2012; Wei et al., 2012). Consequently, continual improvement of available models is essential, but this is contingent upon ongoing validation and evaluation of model performance over a broad range of landscapes and climate types (McCabe et al., 2016). To do this effectively, a diversity of datasets that directly quantify processes represented within these models are required (McCabe et al., 2005). Unfortunately, datasets that directly measure land–atmosphere exchange at the process level are limited (Jana et al., 2016).

Water is composed of a number of stable isotopologues that have sufficient abundance to be measured in atmospheric water vapour ($^1H_2^{16}O$, $^1H^2H^{16}O$, $^1H_2^{18}O$ and $^1H_2^{17}O$). Deviations of water isotope ratios are reported as

$$\delta = \left[\frac{R_{\text{sample}}}{R_{\text{VSMOW}}} - 1\right]‰, \quad (1)$$

where R is the isotope ratio ($^2H/^1H$ or $^{18}O/^{16}O$), and VSMOW (Vienna Standard Mean Ocean Water) is the international standard for reporting water isotope ratios, and these ratios have the potential to evaluate land–atmosphere exchange by discriminating processes based on their isotopic signature (Berkelhammer et al., 2013; Lee et al., 2009; Noone et al., 2013; Risi et al., 2013). Isotopic ratios of water vapour (δ^2H and $\delta^{18}O$) can therefore provide information that is complimentary or even unobtainable when using conventional measurement techniques.

The utility of water isotope ratios for tracing sources of moisture derives from the characteristic equilibrium and kinetic isotopic fractionation that occurs when water undergoes a phase change, causing light water molecules to preferentially accumulate in the vapour phase. Soil moisture is typically enriched in heavy isotopes relative to the ocean (Gat, 1996), so water vapour derived from land surface evaporation is expected to have a different isotopic composition to moisture evaporated from the ocean. This has led to a number of studies using stable isotopes in precipitation to partition oceanic and land-derived sources (Froehlich et al., 2008; Tian et al., 2001). However, land–atmosphere exchange is not restricted to periods of precipitation, and there are relatively few studies examining the role of land–atmosphere exchange on ambient humidity budgets using stable isotope observations of vapour (e.g. Aemisegger et al., 2014; Risi et al., 2013).

In addition to the source of moisture, the magnitude of isotopic fractionation that occurs when water evaporates is related to the liquid surface temperature and humidity gradient between the evaporating surface and atmosphere (Craig and Gordon, 1965). The temperature-dependent equilibrium exchange between liquid and vapour is the largest contributor to isotopic fractionation during evaporation, with the fractionation for δ^2H approximately a factor of 8 greater than $\delta^{18}O$. The effect of kinetic fractionation associated with moisture diffusing from the thin laminar layer of vapour in equilibrium with the water surface to the turbulent atmosphere above is influenced by the relative humidity of the atmosphere and wind speed (Merlivat and Jouzel, 1979). The kinetic fractionation factors for δ^2H and $\delta^{18}O$ are similar, causing the ratio of δ^2H to $\delta^{18}O$ in the evaporating vapour to decrease as kinetic effects increase with decreasing relative humidity. This phenomenon has been observed for evaporative conditions over the Mediterranean Sea (Gat et al., 2003; Pfahl and Wernli, 2009) and the Great Lakes in northern USA (Gat et al., 1994; Vallet-Coulomb et al., 2008).

The D-excess (D-excess $= \delta^2H - 8 \times \delta^{18}O$) parameter (Dansgaard, 1964) quantifies the non-equilibrium isotopic fractionation. A reproducible relationship between the D-excess and relative humidity near the ocean surface has been observed across a wide range of locations (Kurita, 2011; Pfahl and Wernli, 2008; Steen-Larsen et al., 2015; Uemura et al., 2008). Therefore, it has been suggested that for precipitation, D-excess is a good tracer of sea surface evaporative conditions (Masson-Delmotte et al., 2005; Merlivat and Jouzel, 1979). However, this view has recently been challenged due to the role local and regional scale land–atmosphere coupling has in modifying the D-excess of atmospheric humidity over diurnal (Lai and Ehleringer, 2011; Simonin et al., 2014; Welp et al., 2012; Zhao et al., 2014) and synoptic timescales (Aemisegger et al., 2014). As evidence for the role ET plays in modifying the D-excess of water vapour (d_v), a diurnal cycle of d_v near the land surface across a range of land surface types has been observed (Berkelhammer et al., 2013; Simonin et al., 2014; Welp et al., 2012). The diurnal cycle shows higher values during the day, which has been proposed to be driven by entrainment (Lai and Ehleringer, 2011; Welp et al., 2012), local evapotranspiration sources (Simonin et al., 2014; Zhao et al., 2014) and meteorological conditions affecting the D-excess of the evaporative fluxes (d_{ET}) (Welp et al., 2012; Zhao et al., 2014), coupled with low nocturnal values resulting from equilibrium exchange between liquid and vapour pools (Simonin et al., 2014) and dewfall (Berkelhammer et al., 2013). For synoptic scales, Aemisegger et al. (2014) showed that moisture recycling from the land surface had a significant impact on d_v for in situ measurements in Switzerland. These studies have largely relied on isotopic models to assess the contribution of ET fluxes, but a lack of d_{ET} measurements makes it difficult to draw robust conclusions.

The evidence provided by these studies suggest d_v is a tracer of moisture recycling both on diurnal and synoptic timescales, and is influenced by the dynamics of surface moisture budgets in the atmospheric boundary layer (ABL). However, as noted by Welp et al. (2012), ET and entrainment fluxes both increase as the ABL grows through the previous-days residual layer, which can make interpreting the role of local moisture recycling on d_v difficult. To overcome this, Simonin et al. (2014) used a trajectory model to simulate the D-excess of vapour evaporated over the ocean. As the d_v was greater than the modelled oceanic moisture source, it was assumed that high daytime values were supported by local ET fluxes. Zhao et al. (2014) suggested that since, on cloudy days, no diurnal cycle was observed for the d_v, ET fluxes therefore played a dominant role. Whilst these studies provide compelling evidence for the role of ET driving the diurnal cycle of d_v, no measurements of d_{ET} were made. To date the only measurements of d_{ET} have been presented by Huang and Wen (2014) over a maize crop in Northwest China. Interestingly, their direct measurements conflicted with previous interpretations and showed that the d_{ET} invoked a negative

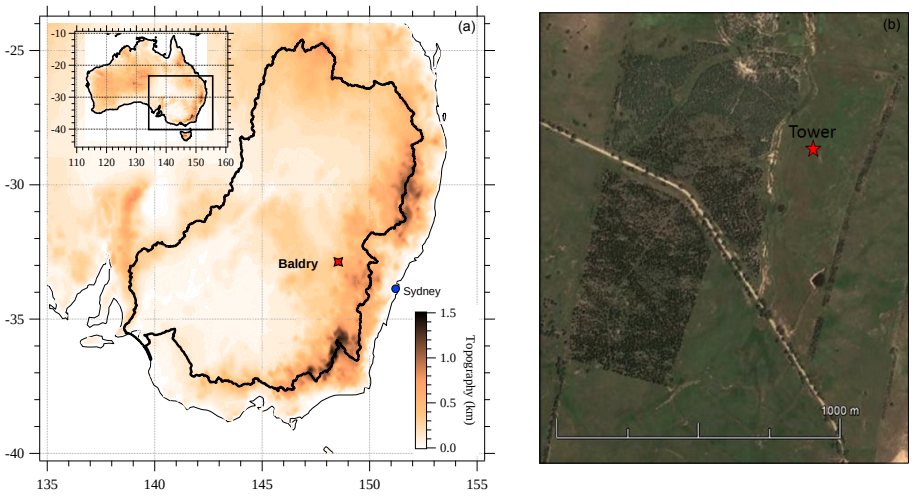

Figure 1. **(a)** Location of the Baldry Hydrological Observatory, with the heavy black border outlining the extent of the Murray–Darling Basin, **(b)** location of the field site used for the campaign, illustrating the semi-arid grassland and adjacent reforested site.

forcing on d_v, even though a strong diurnal cycle of high values during the day and low values at night were observed. In order to better interpret the role of local moisture recycling on the diurnal cycle of d_v, measurements of d_{ET} are required to assess if the negative forcing is consistent across different ecosystems.

The aim of this work is to provide much needed d_{ET} measurements to investigate how ET fluxes modulate the d_v diurnal cycle. To do this, chamber-based measurements of the ET flux isotopic compositions were combined with in situ measurements of water vapour isotope ratios, meteorological and radon concentration observations. The data were collected in a region of the semi-arid Murray–Darling basin in south-eastern Australia. These data represent the first such collection of the δ^2H, δ^{18}O and D-excess in water vapour from this region of Australia. The augmentation of the chamber-based measurements with in situ observations provides a framework to directly assess the role local ET fluxes have on ambient vapour D-excess.

2 Methods

2.1 Site description

During the austral autumn of 2011, a field campaign covering the period 27 April to 11 May was conducted at the Baldry Hydrological Observatory (BHO) (−32.87, 148.54, 460 m a.s.l. – above sea level) located in the central-west of New South Wales, Australia (Fig. 1). The climate of the region is characterised as semi-arid with no clear wet season, a mean annual rainfall of 600 mm, and a mean annual temperature of 24.2 °C (source Australian Bureau of Meteorology, 2016; http://www.bom.gov.au/). The BHO grassland eddy covariance flux tower was the central site of measurements and was located in a natural grassland paddock of dimensions approximately 900 m (north–south) by 300 m (west–east), with a gentle slope decreasing in elevation by approximately 20 m from south-east to north-west. The flux tower was located 650 m from the road to the south and 200 m from a reforested paddock to the west. The forest site to the west and south-west was reforested in 2001 with *Eucalyptus camaldulensis*, *Eucalyptus crebra* and *Corymbia maculata*. At the time of the campaign these trees were approximately 10 m tall. All other adjacent paddocks and most of the surrounding region had similar surface characteristics to the grassland measurement site.

2.2 Water stable isotope analyses

2.2.1 In situ water vapour calibration and sampling

In situ water vapour isotope ratios were monitored using a Wavelength Scanning Cavity Ring Down Spectrometer (WS-CRDS L115-I, Picarro Inc., Sunnyvale, CA, USA), while flux chambers were interfaced to an Off-Axis Integrated Cavity Output Spectrometer (OA-ICOS, DLT100, Los Gatos Research – LGR, Mountain View, CA, USA) to determine the isotopic composition of ET fluxes. Using an automated continuous flow calibration system (built in-house), we simultaneously determined calibration coefficients for both analysers. Calibration experiments were designed to determine the water vapour mixing ratio cross-sensitivity of isotope ratios and linearity of the δ^2H and δ^{18}O measurements. More details on the calibration procedure are found in the Supplement. Due to logistical constraints, the calibration system was not transported into the field, so corrections were determined by compositing multiple calibration experiments run before and after the campaign.

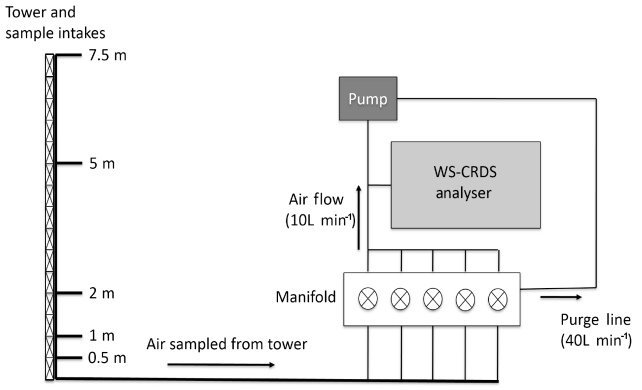

Figure 2. Sampling system for the automated in situ collection and measurement of water vapour isotopes from the tower.

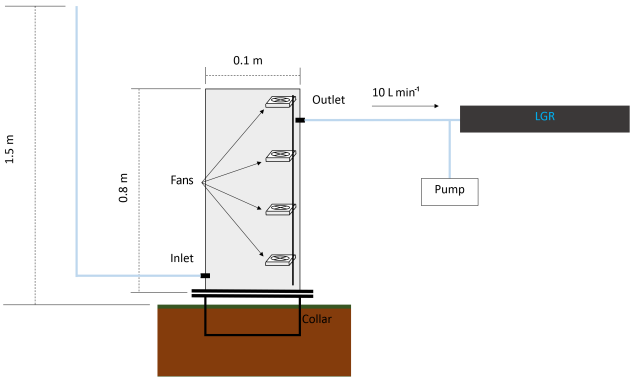

Figure 3. Chamber design used for determining the isotopic compositions of ET fluxes.

During the campaign, a secondary portable calibration system was employed to monitor time-dependent drift of the Picarro analyser (CTC HTC Pal liquid autosampler; LEAP Technologies, Carrboro, NC, USA). Two standards spanning expected water vapour δ^2H (-49.1 and -221.9 ‰) and δ^{18}O (-9.17 and -27.57 ‰) ranges were injected at approximately 18 mmol mol^{-1} on three occasions during the campaign.

The uncertainty of measurements from both isotopic analysers was estimated by applying mixing ratio cross-sensitivity and linearity corrections to all calibration measurements collected prior to, during and after the campaign. For the Picarro instrument, measurement uncertainty was 0.8, 0.2 and 1.9 ‰ for δ^2H_v, $\delta^{18}O_v$ and d_v, respectively. No calibrations were performed for the LGR in field, so the measurement uncertainty was estimated by compositing calibration measurements made before and after the campaign, which were 0.9, 0.4 and 3.3 ‰ for δ^2H, δ^{18}O and d_v, respectively.

Although no calibration experiments were run on the LGR during the campaign, simultaneous in situ measurements were made with the Picarro when chamber measurements were not operated. During the day, average differences were -0.06 ($\pm$2.0), 0.13 ($\pm$0.5) and 0.4 ($\pm$3.3) ‰ for δ^2H, δ^{18}O and d_v, respectively. A comparison of the analysers is shown in Fig. S1 in the Supplement. At night, while the Picarro was able to maintain a steady cavity and optical housing temperature, the LGR cavity temperature dropped by up to 8 °C. In response to the drop in cavity temperature, nighttime LGR measurements of δ^{18}O and d_v, and to a lesser extent the δ^2H, were physically unrealistic and discarded from subsequent analyses. Chamber measurements were therefore restricted to between 09:00 LST (when the LGR cavity temperature had stabilised and in situ measurements were again in agreement with the Picarro) and 17:00 LST (before LGR cavity temperatures began dropping).

A schematic diagram illustrating the sampling design for water vapour is shown in Fig. 2. Half-hourly vertical profiles of humidity and isotopes were sampled by drawing air to the in situ analyser through 10 mm (outside diameter) PTFE tubing, located at five heights on a 7.5 m tower (0.5, 1, 2, 5 and 7.5 m a.g.l.). The instrument was interfaced to a five-inlet manifold that enabled sequential sampling of the different heights. Approximately 20 m of tubing was required to connect the tower inlet to the analyser. A vacuum pump (MV 2 NT, Vacuubrand, Wertheim, Germany) was used to draw air through all inlets to the analyser at a flow rate of 10 L min^{-1}, with the Picarro bleeding off the 0.03 L min^{-1} through its measurement cavity. To avoid condensation, sample tubes and intakes were wrapped in 15 W m^{-1} heat tape, insulated by Thermobreak pipe and placed inside 100 mm PVC pipe. The sample tube temperature was controlled using a resistance thermometer detector coupled to a CAL3300 temperature controller (CAL controls Ltd., Grayslake, IL, USA). The inlets at each height were constructed from inverted funnels with mesh filters. In this study we present block hourly averages of all measurements collected at all heights.

2.2.2 Flux chambers

To separate the isotopic signatures of the ET flux components, flux chambers were deployed on both bare soil and vegetated plots to determine the isotopic signature of the evaporative fluxes. An open chamber was designed with a high volume-to-footprint ratio to avoid the chamber mixing ratio rapidly reaching the dew point temperature (causing condensation) and to minimise impacts on the evaporation environment. A schematic of the chamber design is shown in Fig. 3. Four flanged metal collars were inserted $\sim$ 10 cm into the soil column 2 days before the beginning of the campaign. While this was a short settling time for chamber bases, shallow roots of grass cover within the chamber were largely unaffected. All vegetation was removed from bare soil plots when the metal collars were inserted into the soil. A single chamber cover was constructed out of 4 mm G-UVT Plexiglas (Image Plastics, Padstow, Aus-

tralia), selected for its higher transmittance of UV (ultraviolet) and blue light. The dimensions of the chamber were $0.1 \times 0.1 \times 0.8$ m (width × length × height), with the inlets and outlets at 0.1 and 0.7 m above the surface, respectively. All sampling tubes were 10 mm PTFE. The inlet to the chamber was connected to tubing that drew in air from 1.5 m above the ground surface. The outlet was connected to a flowmeter (VFA-25, Dwyers, Michigan City, IN, USA) that regulated the airflow at $10\,\mathrm{L\,min^{-1}}$ and was driven by a two-stage diaphragm pump. A T-piece was connected to the LGR, which bled off approximately $0.8\,\mathrm{L\,min^{-1}}$. All tubing between the chamber and the analyser were wrapped in heating tape ($15\,\mathrm{W\,m^{-2}}$) and foam insulation. High flow rates were used to combat memory effects modifying the isotopic composition of the vapour within the chamber. Analysis of chamber measurements was conducted on 2–5 min of data, so 2.5–6.25 chamber volumes were exchanged.

To monitor the internal chamber environment, an air temperature and humidity probe (HMP155, Vaisala, Vantaa, Finland) was mounted inside the chamber. To monitor the attenuation of the incoming radiation by the chamber, the photosynthetic flux density was measured (LI-190R, Licor, Lincoln, NE, USA) inside and outside the chamber; 10 s averages of the temperature, relative humidity and photosynthetic flux density were stored in a datalogger (CR1000, Campbell Scientific, Logan, UT, USA). In the Supplement we use these ancillary measurements to assess the impact of observed changes in the chamber environment on the isotopic composition of ET fluxes. The largest contributor to uncertainty caused by changing the evaporative environment was the temperature, although these affects were small compared to the overall variability of the chamber-derived ET isotopic compositions.

2.2.3 Isotopic composition of ET flux from chamber measurements

Mass balance or Keeling-mixing (Keeling, 1958; Wang et al., 2013a) models have been applied to determine the isotopic composition of ET fluxes from chamber measurements (Lu et al., 2017; Wang et al., 2013b). The focus of this work was not to evaluate chamber measurement techniques. Considering that it has been shown that Keeling and mass balance methods give very similar results (Lu et al., 2017; Wang et al., 2013b) we focus on using the Keeling-mixing model, given by

$$\delta_{\mathrm{chamber}} = q_{\mathrm{BG}} \frac{(\delta_{\mathrm{BG}} - \delta_{\mathrm{ET}})}{q_{\mathrm{chamber}}} + \delta_{\mathrm{ET}} \quad (2)$$

where q_{BG} is the water vapour mixing ratio entering the chamber through the inlet and δ_{BG} its isotopic composition, q_{chamber} is the mixing ratio in the chamber and δ_{ET} is the isotopic composition of the ET flux. The δ_{ET} is determined from the intercept of $\delta_{\mathrm{chamber}}$ against $1/q_{\mathrm{chamber}}$. A key assumption of the Keeling method is that the isotopic composition of the background vapour and the evaporation flux remain constant during the chamber measurements. For chamber measurements longer than 5 min, non-linear Keeling plots were commonly observed, indicating a change in isotopic composition of one of the sources of vapour. We therefore restricted the Keeling analysis to a maximum of 5 min after an increase in the concentration was observed by the analyser. Ensuring the linearity of Keeling plots also ensured that the influence of memory effects was minimised. Memory effects would constitute an additional moisture source, violating the two-source assumption of the Keeling methods and reducing Keeling plot linearity. The analysis was also restricted to periods where the H_2O mixing ratio was increasing, so analysis was generally performed on 2–5 min of data. In addition, only chamber measurements where the correlation between $\delta_{\mathrm{chamber}}$ and $1/q_{\mathrm{chamber}}$ was significant ($p < 0.001$) were included in this analysis. A few chamber measurements where obvious non-linearity or very small changes in q_{chamber} occurred were also subjectively removed. Of a total of 105 chamber measurements made from the 4 vegetation plots during the campaign, 99 measurements of the δ^2H_{ET}, and 97 measurements of $\delta^{18}O_{\mathrm{ET}}$ and d_{ET} were retained. For the bare soil plots, 84 of the 86 chamber measurements were retained for the δ^2H_{ET}, and 77 of the $\delta^{18}O_{\mathrm{ET}}$ and d_{ET}. The eight plots were sampled 2 to 4 times each day on all days except the first two days of the campaign, and 2 and 5 May. Sampling was restricted to between 09:00 and 17:00 LST (local solar time) as the large temperature dependence of the LGR at low ambient temperatures limited the accuracy of the chamber measurements.

Results from vegetated plots were used to determine ET flux isotopic compositions and determine how ET influences d_{v}. The bare soil plots were used to determine the isotopic composition of soil evaporation fluxes and to provide an estimate of the isotopic composition of water at the evaporation front. The isotopic composition of the water at the evaporation front (δ_{L}) was determined by rearranging the Craig and Gordon model:

$$\delta_{\mathrm{L}} = \frac{\delta_{\mathrm{E}}(1 - \mathrm{RH}) + \mathrm{RH}\delta_{\mathrm{A}} + \varepsilon + \varepsilon_{\mathrm{k}}}{\alpha} \quad (3)$$

where the isotopic composition of the evaporation flux (δ_{E}) is taken from the bare soil chamber measurements, relative humidity (RH) normalised to the surface temperature determined from infrared surface temperature measurements (Sect. 2.3), and the ambient vapour isotope composition (δ_{A}) determined from Picarro in situ measurements. Equilibrium fractionation and enrichment factors (α, $\varepsilon = (\alpha - 1)$‰) were calculated from the surface temperature measurements using the equations of Horita and Wesolowski (1994), while the kinetic enrichment factors (ε_{k}) were determined as in Gat (1996), but using the parameterisation of the exponent of the diffusion coefficients described by Mathieu and Bariac (1996) and the diffusion coefficients determined by Merlivat (1978).

2.2.4 Isoforcing of ET

The isotopic composition of the near-surface atmospheric water vapour is modified by surface ET fluxes. The impact of ET fluxes on surface vapour isotopes varies over diurnal timescales with the strength of vertical mixing in the ABL or over synoptic timescales as background moisture conditions change. The magnitude and isotopic composition of the ET flux as well as the amount of water vapour in the atmosphere also have an influence. The ET isoforcing (I_{ET}) represents a useful quantity to study the influence of ET fluxes on the surface vapour and is defined as

$$I_{ET} = \frac{F_{ET}}{H_2O}(\delta_{ET} - \delta_A), \quad (4)$$

where F_{ET} is the ET flux in mol m^{-2} s^{-1}, H_2O is the ambient mixing ratio in mol-air mol-H_2O^{-1} measured by the local meteorological tower, and δ_{ET} and δ_A are the isotopic compositions of the evaporation flux and ambient water vapour, respectively (Lee et al., 2009).

For each chamber measurement, a surface isoforcing was calculated for δ^2H, δ^{18}O and D-excess from the determined ET isotopic composition, as well as the hourly averaged ET flux, mixing ratio and δ_A values. The importance of surface fluxes modifying surface vapour isotope composition was investigated for diurnal and synoptic timescales.

2.2.5 Plant and soil sampling

Grass samples were collected three times a day for the duration of the campaign. They were sampled randomly within 100 m of the instrumentation. Each sample consisted of approximately 10 grass leaves, which were placed in 12 mL Exetainer vials (Labco, Ceredigion, UK). The grass samples were assumed to represent bulk leaf water. Soil samples were collected every 2 days throughout the campaign by sampling from the top 5 cm of the soil column. They were collected in 50 mL glass bottles. Soil and plant samples were stored in a fridge (4 °C), before using the distillation method of West et al. (2006) to extract liquid water samples that were analysed on a Delta V Advantage Isotope Ratio Mass Spectrometer (Thermo Fisher Scientific Corporation, Massachusetts, USA). For δ^2H analysis, water samples were introduced into a H-device containing a chromium reactor, while for the δ^{18}O analysis, water samples were equilibrated with CO_2 on a Gas Bench II chromatography column (Thermo Fisher Scientific Corporation, Massachusetts, USA) before being transferred to the Isotope Ratio Mass Spectrometer (IRMS) for analysis.

2.3 ET fluxes and meteorological measurements

To measure ET fluxes, an eddy covariance system comprising a Campbell Scientific 3-D sonic anemometer (CSAT-3, Campbell Scientific, Logan, UT, USA) along with a Licor 7500 (Li-7500, Licor Biosciences, Lincoln, NB, USA) analyser was installed at an elevation of 2.5 m. The system was located approximately 10 m from the stable isotope observation tower and sampled at 10 Hz, with flux averages output at 30 min intervals. The ET fluxes from the eddy covariance tower are used to quantify the isoforcing of ET on the overlying atmosphere.

A meteorological tower was co-located with the eddy covariance system, providing complementary data to aid in the interpretation of measurements. The tower comprised a Kipp and Zonen CNR4 radiometer, Apogee infrared surface temperature, RIMCO rain gauge, Vaisala HMP75C temperature and humidity probe, RM Young wind sentry (wind speed and direction), Huskeflux ground heat flux plate and Vaisala BaroCap barometric pressure sensor. Both meteorological tower data and eddy covariance data were inspected visually to detect and remove spikes. The low-frequency eddy covariance data (30 min resolution) were corrected for coordinate rotation (Finnigan et al., 2003) and density effects (Leuning, 2007) using the PyQC software tool (available from http://code.google.com/p/eddy).

2.4 Radon-222 measurements

The naturally occurring radioactive gas radon (^{222}Rn) is predominantly of terrestrial origin and its only atmospheric sink is radioactive decay (Zahorowski et al., 2004). The surface flux density of radon is relatively constant in space and time, and since the half-life is much greater than ABL-mixing timescales, it is an ideal tracer of vertical mixing strength within the ABL (Chambers et al., 2015c; Griffiths et al., 2013; Williams et al., 2010). Hourly radon concentrations were measured by an Alpha Guard (Saphymo GmbH, Frankfurt, Germany) placed in a $\sim$ 20 L enclosure. The enclosure was purged at $\sim$ 15 L min^{-1} with a vacuum pump (2107 Series, Thomas, Wisconsin, USA) that sampled from a height of 2 m through 10 mm (outside diameter) PTFE tubing. Radon measurements were used to aid the interpretation of the diurnal variations in vertical mixing (see Griffiths et al., 2013).

3 Results

3.1 Meteorological observations

The last rain event was 10 days prior to the campaign, after which clear skies saw the soil dry to a moisture content close to minimum values observed for the site (Fig. 4). The meteorological and radon measurements shown in Fig. 5 indicate the 2-week campaign was conducted under predominantly calm meteorological conditions. In the middle of the campaign (2 May), a cold front moved across south-eastern Australia, producing cloudy conditions and 1.4 mm of precipitation at the site. No change in soil moisture was observed over the 0–10 cm soil layer following the rain event.

Wind directions were variable during the campaign (see Fig. S2a and b). Figure S3 shows that from 27 to 30 April,

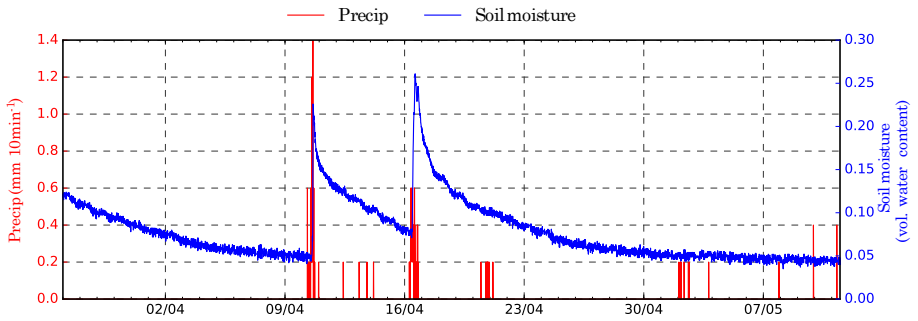

Figure 4. Precipitation and 0–10 cm soil moisture for the month leading up to and including the field campaign.

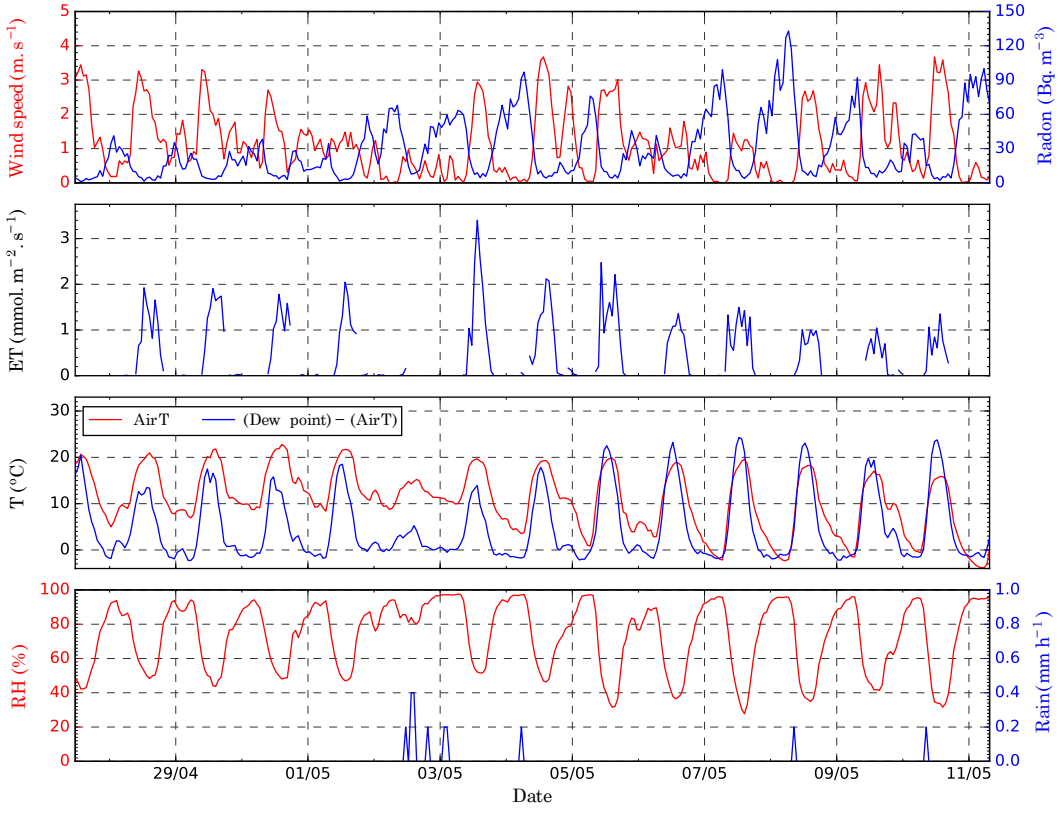

Figure 5. Meteorological and radon measurements collected throughout the field campaign. Meteorological measurements are block hourly averages calculated from 15 min observations. Small rain events on 4, 8 and 10 May were most likely dewfall rather than precipitation.

dominant daytime wind directions were mainly from the east. After 3 May winds were from the south, except on 7 and 8 May when the wind was from the west and had a fetch from the adjacent forest. At other times the fetch did not overlap the forested site. Daily maximum temperatures on clear days ranged from 16 to 23 °C, whilst nighttime minimum temperatures fell to between 8 and −4 °C. From 7 May onwards nocturnal temperatures fell below zero. On clear nights the surface temperature fell below dew point temperature, indicating dewfall. Apart from the night of 27–28 April and the cloudy nights between 1 and 3 May, the surface temperature fell below dew point temperature and dew or frost was observed in the morning, although heavier from 7 May onwards.

Radon concentrations were low during the day, when the convective boundary layer reached its maximum height, and high at night, when radon emissions were confined within the shallow nocturnal boundary layer. The accumulation at night was variable indicating a varying degree of nocturnal stability, mixing depth and occurrence of transient mixing events (Griffiths et al., 2013). There was general agreement between high nocturnal radon concentrations and low wind

speeds, but no direct relationship. The lack of a direct relationship indicates that radon can provide additional information about nocturnal mixing and surface exchange that compliments standard meteorological measurements (Chambers et al., 2015a, b; Williams et al., 2013).

ET fluxes were in general quite low, reflecting the low soil moisture content. The ET flux did show a marked increase the day after the small rain event on 2 May and noticeably smaller fluxes were observed after the first night frost was observed. The health of the grass visibly deteriorated from 7 May, coinciding with frost formation.

3.2 Relationship between δ^2H and δ^{18}O of the different water pools

A summary of the isotopic composition of all observed and modelled water pools are presented in Fig. 6. The local Meteoric Water Line (MWL) (Hughes and Crawford, 2013) is to the left of the global MWL (Craig, 1961), illustrating the characteristically high D-excess of precipitation in the region (Crawford et al., 2013). Ambient vapour observations aligned closely with the local MWL, but with a distribution that fell both to the left and right of the local MWL. Alignment between observations and the MWL show that equilibrium fractionation was the dominant process modifying δ^2H and δ^{18}O in water vapour, while non-equilibrium kinetic processes shift observations away from the MWL and are more easily observed for d_v measurements.

Plant and soil water pools were enriched relative to the vapour and distributed to the right of the MWL, indicating evaporative enrichment. Soil water isotopes at the evaporation front (δ_L) were very enriched and had lower D-excess values (50 ± 12, 31 ± 3.8 and -131 ± 22 ‰ for δ^2H, δ^{18}O and D-excess) relative to the average soil moisture between 0 and 5 cm (-15 ± 4.2, 2.6 ± 2.5 and -36 ± 17 ‰ for δ^2H, δ^{18}O and D-excess). Low D-excess and enriched isotopes indicated large evaporative enrichment under non-equilibrium conditions consistent with the δ^{18}O soil profile measurements of Dubbert et al. (2013) and the δ^2H profiles of Allison et al. (1983). The uncertainty of modelled isotope values was the most sensitive to parameterisation of the Craig–Gordon model. Changing the diffusion coefficient exponent (n) had the greatest impact on modelled soil water ($n = 0.66$, 42.7 ± 12, 21.8 ± 3.8 and -130.8 ± 22 ‰). However, changing parameterisation did not change the conclusion that soil moisture at the evaporation front was heavily enriched with very low D-excess values.

ET flux isotopic compositions from vegetated chambers were enriched relative to vapour and distributed to the right of the MWL (slope = 3.2). Similar isotopic compositions were measured from bare soil and vegetated chambers. Mean and standard deviations (1σ) for vegetated and soil chambers were -47.1 (± 13) and -50.2 (± 11) for δ^2H, -5.03 (± 3.8) and -6.3 (± 2.7) ‰ for δ^{18}O, and -6.3 (± 23) and -0.12 (± 15) ‰ for D-excess, respectively. The similar ET isotopic

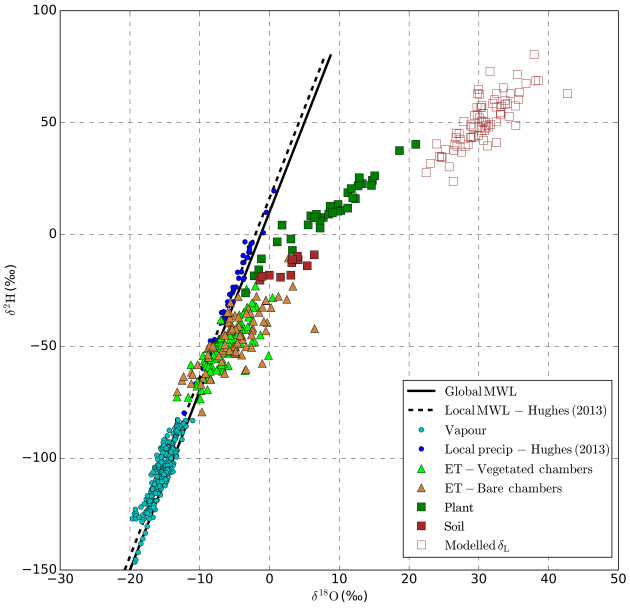

Figure 6. Relationship between δ^2H and δ^{18}O for observed and modelled water pools. Linear regressions are shown for local and global meteoric water lines (MWL). Data from Hughes and Crawford (2013) are for monthly cumulative rainfall samples between 2005 and 2008.

composition from bare soil and vegetated chambers could indicate soil evaporation was the dominant process contributing to total ET. However, as pointed out in the discussion (Sect. 4.3), convergence of soil evaporation and transpiration isotope compositions as the soil evaporation source becomes progressively enriched (and D-excess lower), probably makes it difficult to identify the dominant process from these observations. Nevertheless, since the last significant rain event prior to the campaign, progressive reduction of D-excess of moisture at the evaporation front, and to a lesser extent in the 0–5 cm layer, caused low D-excess of overall ET fluxes compared to d_v. This would indicate that ET imposes a negative forcing on d_v.

Temporally, a clear trend was not observed for ET isotopic compositions over the measured portion of the diurnal cycle or over the campaign. No measurements were made at night or during the rapidly changing conditions of the morning transition, which may have led to our data missing some observed changes in ET isotope compositions.

3.3 In situ water vapour isotopes and ET isoforcing

Observed water vapour mixing ratios and stable isotope compositions are shown in Fig. 7. δ^2H and δ^{18}O variability was similar, reflecting changes in both the synoptic and local meteorology. Prior to the rain event (2 May), relatively moist conditions (higher H_2O mixing ratios) were observed as air was transported from the warmer ocean off the east coast of Australia (see wind direction in Fig. S3). After 5 May, trans-

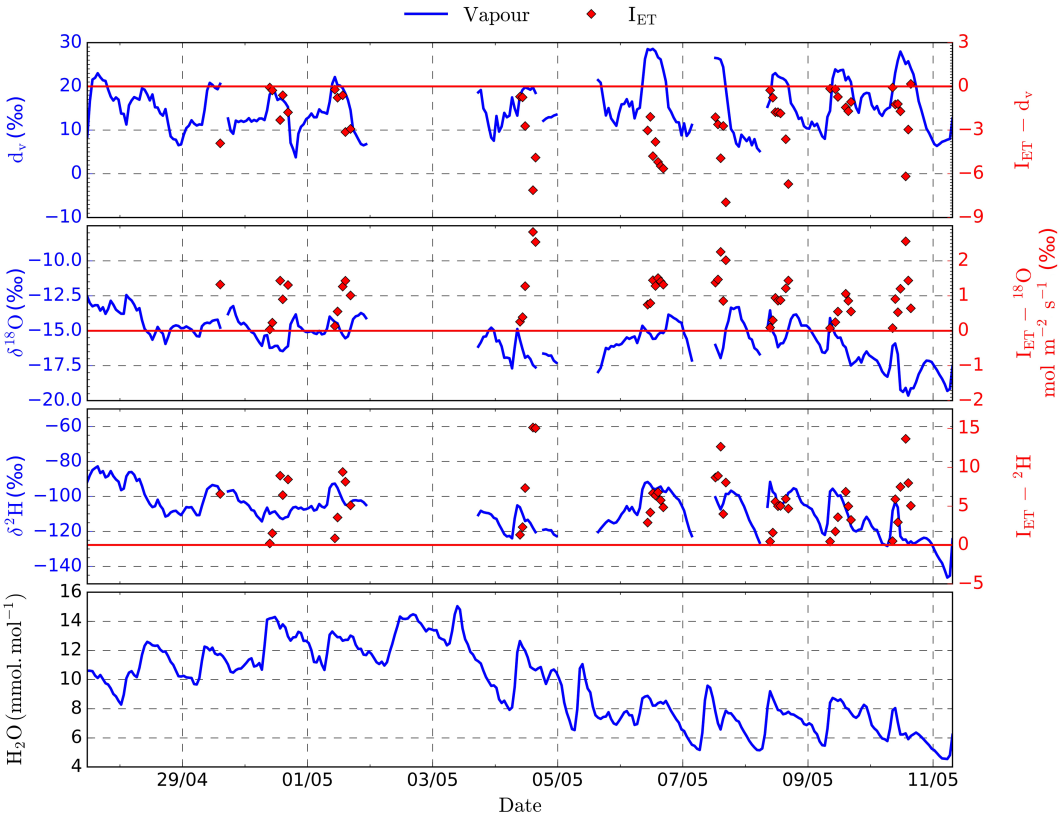

Figure 7. Time series of hourly water vapour mixing ratio, isotopic composition and ET isoforcing (I_{ET}).

port of air masses from the colder sea surface south of continental Australia brought drier conditions to the site (lower H_2O mixing ratios). Moisture source regions were confirmed by backward air trajectories calculated using the Stochastic Time-Inverted Lagrangian Transport Model (STILT; Lin et al., 2003, not shown). These two time periods are hereinafter referred as the "wet period" (before 2 May) and the "dry period" (after 5 May). The wet period coincided with more enriched isotopes and less diurnal variability. In the later part of the campaign, a reproducible diurnal cycle for δ^2H and δ^{18}O was observed (see Fig. 8 for diurnal composites), presenting a sharp increase at sunrise before decreasing from mid-morning (when vertical mixing increased) until the next sunrise. These observations emphasise the complex relationship between stable isotope observations in water vapour and both local- and synoptic-scale meteorology.

The d_v dataset showed a robust diurnal cycle of high values during the day and low values at night, consistent with what has been observed across a growing number of locations (Bastrikov et al., 2014; Berkelhammer et al., 2013; Simonin et al., 2014; Welp et al., 2012; Zhao et al., 2014). Wet period daytime d_v values were on average lower than those observed for the dry period. Nocturnal d_v was consistently lower during the night, but variable from night to night and across individual nights, with no clear difference observed between wet and dry periods. Contrasting daytime measurements of wet and dry periods indicate a role of large-scale processes, whilst the lack of contrast for nocturnal observations shows the importance of local processes.

The I_{ET} was always positive for δ^2H and δ^{18}O and mostly negative for D-excess, but showed large variability across individual days (Fig. 7). I_{ET} was most sensitive to the magnitude of the ET fluxes, producing the greatest forcing on ambient vapour in the middle of the day. The I_{ET} time series did not correspond to temporal variability of vapour δ^2H, δ^{18}O or D-excess. δ^2H and δ^{18}O often decreased during the day while I_{ET} was positive. Whilst the high d_v values observed during the day were associated with negative isoforcing, over the course of the campaign the highest daytime d_v values did not correspond to the least negative I_{ET}. These observations illustrate that local ET fluxes were not overly important for day-to-day and diurnal d_v trends.

The level of agreement between the analysers presented some uncertainty in calculating the D-excess isoforcing. The sign of the isoforcing is dependent on the difference between d_v and d_{ET} (Eq. 8). In some cases this difference was small and within the range of agreement between the two analysers. While this caused problems for accurate calculation of the absolute values of D-excess isoforcing, for all chamber measurements passing our quality control requirements, D-

Table 1. Correlation between meteorological variables and the isotopic composition of water vapour. Values outside the brackets are statistics for the hourly observations. Inside the brackets are correlation statistics for average values calculated between 11:00 and 15:00 LST, hence representing activity during a convective boundary layer. Significant correlation are shown in bold; $p < 0.001$ for hourly observations and $p < 0.05$ for the daytime averages (due to the smaller number of points).

		T	RH	ET	H_2O	I^*_{ET}
δ^2H	Slope	**0.83** (0.51)	**–0.17** (0.23)	1.4 (6.1)	**2.1** (0.85)	−1.1 (**–3.0**)
	Intercept	**–120** (−140)	**–95** (−110)	−110 (−110)	**–110** (−130)	−99 (**–83**)
	R^2	**0.24** (0.13)	**0.09** (0.02)	0.001 (0.04)	**0.2** (0.04)	0.2 (**0.45**)
	p	< **0.001** (0.3)	< **0.001** (0.7)	0.32 (0.6)	< **0.001** (0.5)	0.002 (**0.05**)
$\delta^{18}O$	Slope	**0.046** (0.44)	−0.01 (−0.01)	−0.37 (1.8)	**0.27** (0.29)	−0.7 (−1.9)
	Intercept	**–16** (−24)	−16 (−20)	−15 (−18)	**–18** (−19)	−15 (−14)
	R^2	**0.04** (0.30)	0.004 (0.2)	0.02 (0.16)	**0.2** (0.2)	0.14 (0.32)
	p	< **0.001** (0.08)	0.26 (0.19)	0.05 (0.26)	< **0.001** (0.15)	0.008 (0.11)
d_v	Slope	**0.51** (**–1.4**)	**–0.21** (**–0.52**)	0.01 (**–0.16**)	0.15 (**–1.3**)	−1.4 (−2.4)
	Intercept	**–9.9** (**48**)	**31** (**44**)	−15 (**–18**)	14 (**35**)	21 (20)
	R^2	**0.40** (**0.48**)	**0.62** (**0.74**)	0.22 (**0.30**)	0.004 (**0.71**)	0.06 (0.08)
	p	< **0.001** (**0.02**)	< **0.001** (< **0.01**)	0.05 (**0.01**)	0.26 (< **0.01**)	0.01 (0.44)

* Isoforcing correlations were calculated for simultaneous vapour and chamber measurements. Hourly averaged values were used for both.

excess decreased with concentration. This indicates that for all measurements, the D-excess isoforcing was negative.

3.4 Relationship between water vapour isotopes and local meteorology

The relationships between local meteorological variables and water vapour isotopes were examined to interpret the role of local processes (Table 1). Regression statistics are shown for both hourly observations and average daytime values (between 11:00 and 16:00 LST). Selecting daytime measurements removes variability associated with transition between the stable nocturnal and daytime convective boundary layer, as well as nocturnal periods when local surface equilibrium exchange and dewfall affect vapour isotope compositions. Correlations determined using only measurements in the middle of the day therefore provide a better indicator of how local meteorology and ET isotopic composition modified ambient water vapour isotope ratios from day to day.

Correlations calculated with hourly data were weak for $\delta^{18}O$ and δ^2H. Only correlations with air temperature ($R^2 = 0.24$ and 0.04, respectively) and mixing ratio ($R^2 = 0.2$ for both isotopes) were significant, and δ^2H also showed a weak correlation with RH ($R^2 = 0.09$). For daytime observations, only δ^2H showed a significant correlation with daytime I_{ET} ($R^2 = 0.45$, $p < 0.05$), but the slope was negative in contrast to positive isoforcing. The weak relationships with local meteorology indicate the importance of larger-scale precipitation processes and atmospheric mixing occurring as moisture was transported to the site.

As the diurnal cycle for d_v was consistent with growth and decay of the ABL, strong relationships were observed with air temperature and RH for the hourly observations. While the local air temperature and RH could modify d_{ET} on diurnal timescales and in turn local d_v, the chamber measurements showed relatively constant d_{ET}. These correlations therefore result from the coincident diurnal variation of the d_v, RH and air temperature.

Daytime average d_v showed significant correlations with the air temperature, RH, ET flux and mixing ratio. The relationship with ET fluxes was weak ($R^2 = 0.3$) and positive, but as negative D-excess isoforcing was observed, a negative relationship would be expected. Likewise, the slope between air temperature and d_v was negative, counter to what theory would predict for local or remote moisture sources. The strongest relationship was observed with daytime RH ($R^2 = 0.74$), which had a negative slope ($-0.52\,‰\,\%^{-1}$) consistent with an inverse relationship between d_v and RH for a large unchanging evaporation source. The strong relationship of d_v with the daytime RH could indicate an important role for the evaporation conditions at remote moisture sources, as is discussed below in Sect. 4.2.

3.5 Diurnal variability of vapour isotopes

Diurnal composites were divided into dry and wet periods and are shown in Fig. 8. At sunrise (approximately 06:30 LST) surface heating initiated vertical mixing, shown by the radon concentration maximum, causing temperature and ET flux to increase and RH to decrease. Weak vertical mixing immediately after sunrise and injection of ET into the still shallow surface layer caused near-surface humidity to increase. Similarly, for δ^2H and $\delta^{18}O$, the observed spike immediately after sunrise was likely caused by ET fluxes with an enriched heavy isotope composition, possibly from re-evaporation of dewfall. During the dry period, vapour δ^2H

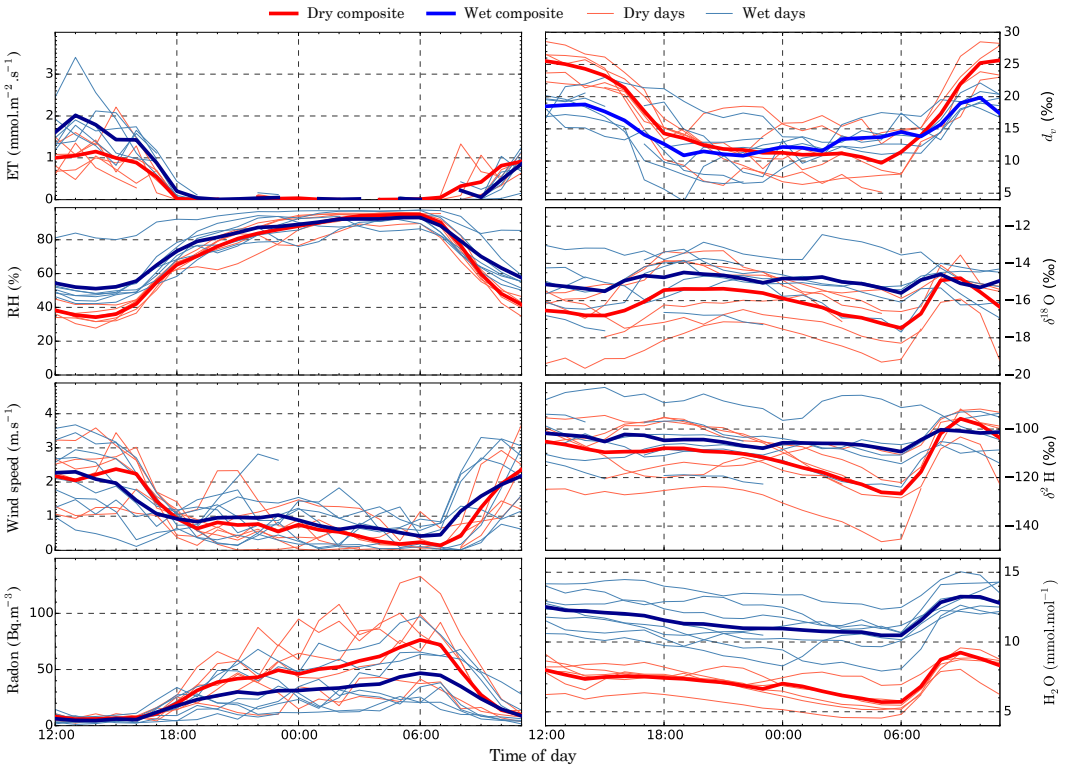

Figure 8. Data plotted by time of day and divided into dry and wet periods (see text in Sect. 3.5). Diurnal composites are shown for dry (red) and wet (blue) periods.

and δ^{18}O increased more steeply, caused by the combination of a shallower surface layer observed at the start of the morning transition, shown by higher radon concentrations, and more dewfall on the surface providing a greater initial evaporation source. Rapidly decreasing radon concentrations during this morning ABL transition caused by vigorous vertical mixing entraining air from the residual layer of the previous day diluted ET fluxes and caused the δ^2H, δ^{18}O and the mixing ratio to first stabilise and then decrease. ET fluxes rapidly increased as the ABL grew, but were not large enough to offset the dilution by dry air being mixed down from above or stop depletion of surface δ^2H and δ^{18}O.

The d_v also increased after sunrise, but aligned more closely to when strong vertical mixing commenced, as shown by the close agreement with radon concentrations. The D-excess isoforcing was negative, evidence that d_v increased from encroachment mixing as the new mixed layer grew in depth and not ET fluxes. The dry period showed a greater increase in d_v during the morning transition, likely the result of higher d_v in background water vapour and greater differences between the d_v of the residual and nocturnal layer.

In the afternoon, d_v decreased back to values similar to those observed prior to sunrise, with a simultaneous decrease in solar insolation, ET and a decay of convective mixing. Radon shows how reduction in vertical mixing causes the concentration of tracers emitted from the surface to increase. So while ET decreased, small fluxes were still observed well after 18:00 LST, when large changes in δ^{18}O and d_v were observed. Hence, as the I_{ET} was positive and negative for δ^{18}O and D-excess, respectively, small ET fluxes into a poorly mixed surface layer may have led to observed changes.

During the night, dewfall caused δ^2H and δ^{18}O to decrease as heavy isotopes were removed in condensation, especially during the dry period when greater surface cooling was observed. However, dew formation is an equilibrium processes and therefore did not affect d_v. Composites of dry and wet period nocturnal d_v measurements do not show clear nocturnal trends, but individual nights showed considerable variability. A regression of nocturnal d_v with radon concentrations produced a significant negative relationship ($p < 0.001$, $R^2 = 0.31$), indicating that atmospheric stability has some control over nocturnal d_v. High radon is associated with the most stable atmospheres, enhancing the effect of surface exchange in the early evening. Low radon, on the other hand, is associated with periods of atmospheric turbulence in which moisture above the nocturnal inversion with a high d_v is mixed down towards the surface.

4 Discussion

As has been previously observed (Steen-Larsen et al., 2013; Welp et al., 2012) and predicted by isotopic models (Gat, 1996), our observations showed water vapour δ^2H and δ^{18}O are controlled by different atmospheric and hydrological processes than d_v. The diurnal cycle was the dominant mode of variability for d_v, consistent with previous studies for a range of ecosystems (Simonin et al., 2014; Welp et al., 2012; Zhao et al., 2014). However, results also showed that D-excess variability was controlled by local meteorological conditions and surface exchange at night, ABL growth and decay during transitional periods between the nocturnal and convective ABL, and larger-scale processes in the middle of the day.

4.1 Entrainment and the d_v diurnal cycle

The radon measurements showed that when the depth of the ABL was rapidly changing through the morning and evening transitions, entrainment from the residual layer and ET fluxes into a rapidly decaying convective boundary layer caused the observed d_v diurnal cycle. Between these transitions, when mixing extends to the capping inversion, entrainment fluxes introduce an additional moisture source from the free troposphere that could modify surface vapour isotopic compositions. Air above the ABL is drier and moisture is more depleted than at the surface. Drying and depleting trends for water vapour, δ^2H and δ^{18}O throughout the day, particularly during the dry period (Fig. 8), indicate an important role for entrainment from the free troposphere. Whether this moisture flux impacts on d_v is less clear, as it remained reasonably stable once a maximum was reached after the morning transition period. The sign of the isoforcing of moisture entrained from the free troposphere is uncertain, as few free tropospheric d_v measurements exist (He and Smith, 1999; Samuels-Crow et al., 2014). Nevertheless, d_v values did not show a clear trend until vertical mixing began decaying later in the afternoon; therefore, free tropospheric d_v probably has a similar value to moisture already residing in the ABL.

4.2 Remote hydrometeorological processes

While the main focus of this study was to examine the role of local land–atmosphere exchange for the diurnal variability of d_v, the synoptic context of measurements warrants further examination for comparison against previous studies of d_v diurnal cycles. The slope between daytime RH and d_v ($-0.52\,‰\,\%^{-1}$, Table 1) was similar to those determined for measurements over the Mediterranean Sea and different ocean basins (between -0.43 and $-0.53\,‰\,\%^{-1}$) (Kurita, 2011; Pfahl and Wernli, 2008; Steen-Larsen et al., 2014, 2015; Uemura et al., 2008). Aemisegger et al. (2014) showed that this robust relationship is not restricted to coastal locations or measurements over the ocean surface. Using a trajectory model to investigate continental moisture recycling in Europe, they found a similar relationship between d_v and RH of remote moisture sources during the cold season ($-0.57\,‰\,\%^{-1}$), but not for warm season observations. They concluded moisture recycling is weakest during winter, causing d_v to retain the signature of the RH of oceanic moisture sources, while in summer moisture recycling increased and attenuated the relationship. Similarities with their winter data indicate that our daytime d_v measurements were at least partly determined by RH at the oceanic moisture source.

Along an air masses back trajectory, entrainment fluxes from the free troposphere could be a major driver of daytime d_v variability. Mixing of warm dry air down to the surface, presumably with a relatively high D-excess (He and Smith, 1999; Samuels-Crow et al., 2014), would give the same negative relationship between d_v and RH observed here. However, for a strong relationship between d_v and RH, there must be a dominant moisture source. For the fraction of entrained air in the ABL to cause the strong linear relationship, the D-excess of vapour and RH in both the ABL and free troposphere must be reasonably constant, as in a two-source mixing model. Considering the variability of synoptic-scale weather patterns observed (Sect. 3.1), this seems unlikely. Thus, while we cannot definitively rule out the importance of entrainment along back trajectories, it seems more likely that the d_v–RH relationship was derived from a large unchanging moisture source such as the ocean.

A practical application of the d_v–RH relationship introduced by Aemisegger et al. (2014) was to determine the D-excess of the liquid moisture source. Based on the closure assumption of Merlivat and Jouzel (1979), it was shown when RH is 100 %, d_v is equal to the D-excess of the liquid moisture source. If no further kinetic fractionation or mixing of vapour with a different d_v–RH occurred between the point of evaporation and measurement location, extrapolating the regression between d_v and RH to 100 % RH gives an estimate of moisture source D-excess. For our measurements, a value of $-8\,‰$ was determined, remarkably similar to the D-excess determined for ocean water off the east coast of Australia by Xu et al. (2012) using a global ocean model. In contrast to recent literature (Simonin et al., 2014; Welp et al., 2012; Zhao et al., 2014), this suggests that although the common diurnal cycle was observed, daytime observations are potentially a tracer of RH at the oceanic moisture source, but it is likely restricted to periods when moisture recycling is weak.

Whilst we have shown a relationship between the RH and d_v consistent with an oceanic vapour source, the consistency of the relationship over longer time periods is uncertain. Indeed, it may be the reason why we show a strong relationship, whereas the study of Welp et al. (2012) did not for six mid-latitude sites in China and the USA, where longer datasets were available. As pointed out earlier, lowers slopes and weaker relationships result from stronger moisture recycling, which indicates moisture recycling and soil moisture state may be the most important variable controlling the relationship between d_v and RH. Here we present data from after

an extended dry period, where the dominant moisture source is the ocean surrounding the Australian continent. So during wetter periods, an increase in the local and remote moisture recycling probably weaken the relationship between local d_v and RH (Aemisegger et al., 2014). However, for locations such as semi-arid Australia where extended dry periods prevail, the relationship between d_v and RH may be reasonably robust and prevail as a tracer of oceanic evaporative environments.

4.3 Controls of d_{ET}

The chamber d_{ET} measurements showed ET fluxes imposed a negative isoforcing on d_v, in contrast to interpretations in previous studies investigating d_v variability on diurnal timescales (Simonin et al., 2014; Zhao et al., 2014). However, it is expected that the sign and magnitude of the D-excess isoforcing would vary both spatially and temporally, in particular with the soil moisture state. After a rain event, soil moisture D-excess would decrease following a pseudo-Rayleigh process (Barnes and Allison, 1988). Therefore, immediately after a rainfall event, d_{ET} would be higher and probably impose a positive isoforcing. Here the negative d_{ET} caused the d_v to decrease rapidly as convective mixing shut down. When isoforcing is positive after a rain event, the diurnal cycle observed here and elsewhere may therefore not be observed. Although equilibration between liquid and vapour pools, as eluded to by Simonin et al. (2014), may still help maintain observed trends. As soil dries, a tipping point when the ET fluxes switch from positive to negative isoforcing will be observed. This has implications for studies attempting to use d_v as a tracer of continental moisture recycling, as the large spatial variability of rainfall and the associated soil moisture state would lead to large spatial and temporal variability for d_{ET}. Although, the strongest moisture recycling is expected for wet soils when d_{ET} is higher, variability in d_{ET} may still be important.

Relative magnitudes of evaporation and transpiration fluxes are important for d_{ET}, as the two processes could have different D-excess values and could vary strongly between precipitation or irrigation events. The classical view of ET isotope fluxes is that transpiration has an isotopic composition closer to the source moisture than evaporation, and therefore a higher D-excess. However, greater fractionation of the evaporation source pool causes its D-excess value to decrease over time, causing the D-excess of the fluxes to converge. The impact of converging isotopic signatures of ET component fluxes on moisture recycling would depend on the land surface type, but would constitute an important variable influencing the D-excess of local and remote moisture recycling. Further studies investigating how ET partitioning and drying of soil moisture reservoirs following irrigation or precipitation events would lead to a better understanding of how moisture recycling influences the ambient d_v on continental and local scales.

5 Conclusions

To determine how local ET fluxes modified water vapour D-excess, in situ observations were collected in a semi-arid region of south-eastern Australia. The diurnal cycle exhibited high values during the day and low values at night, reflected findings from previous studies. With chamber-based measurements of isotopic compositions in evaporative fluxes, it was shown that local ET fluxes exhibited a negative forcing on the ambient water vapour D-excess that could not explain the high daytime values. A strong negative relationship was observed between the locally measured relative humidity and vapour D-excess during the daytime, consistent with relationships observed for oceanic moisture sources. During the evening transition, collapse of the convective boundary layer and small ET fluxes with negative D-excess isoforcing were responsible for lowering the D-excess of water vapour near the surface. In addition, a negative nocturnal correlation between D-excess in water vapour and radon concentrations indicated transient nocturnal mixing events shifted the D-excess back towards the higher values observed during the day, with the most stable (least turbulent) nights producing the lowest D-excess values. In the morning, encroachment and entrainment of high D-excess air from above caused D-excess of surface vapour to increase back to the synoptic values.

Overall, it was found that the magnitude of the D-excess diurnal cycle was controlled predominantly by interplay between synoptic forcing and local ABL processes and was modified further by nocturnal surface exchange processes and turbulent mixing. The low D-excess of the ET fluxes determined from flux chambers in this study illustrated that the impact of large-scale moisture recycling may be both spatially and temporally variable, depending on the soil moisture state. This has implications for studies using D-excess to investigate moisture recycling.

6 Data availability

For access to the data used in this paper contact Stephen Parkes by email (stephen.parkes@kaust.edu.sa).

The Supplement related to this article is available online at doi:10.5194/hess-21-533-2017-supplement.

Acknowledgements. Stephen Parkes was supported by the Atmospheric Mixing and Pollution Transport (AMPT) project at the Australian Nuclear Science and Technology Organization (ANSTO) and the King Abdullah University of Science and Technology. The Baldry Hydrological Observatory field campaign was supported by Australian Research Council Discovery grants DP0987478 and DP120104718. Matthew McCabe acknowledges the support of the King Abdullah University of Science and

Technology. We thank Peter Graham, Cecilia Azcurra, Jin Wang and Yingzhe Cai for their assistance during the campaign. We also appreciate the support of Diana and Jason Tremain for access to the Baldry Hydrological Observatory and surrounding farmland, Chris Dimovski for performing plant and soil water extractions and Barbara Neklapilova analysis of plant and soil water samples.

Edited by: C. Stumpp
Reviewed by: two anonymous referees

References

Aemisegger, F., Pfahl, S., Sodemann, H., Lehner, I., Seneviratne, S. I., and Wernli, H.: Deuterium excess as a proxy for continental moisture recycling and plant transpiration, Atmos. Chem. Phys., 14, 4029–4054, doi:10.5194/acp-14-4029-2014, 2014.

Allison, G. B., Barnes, C. J., and Hughes, M. W.: The distribution of deuterium and ^{18}O in dry soils 2. Experimental, J. Hydrol., 64, 377–397, doi:10.1016/0022-1694(83)90078-1, 1983.

Australian Bureau of Meteorology: http://www.bom.gov.au, last access: 2016.

Barnes, C. J. and Allison, G. B.: Tracing of water movement in the unsaturated zone using stable isotopes of hydrogen and oxygen, J. Hydrol., 100, 143–176, doi:10.1016/0022-1694(88)90184-9, 1988.

Bastrikov, V., Steen-Larsen, H. C., Masson-Delmotte, V., Gribanov, K., Cattani, O., Jouzel, J., and Zakharov, V.: Continuous measurements of atmospheric water vapour isotopes in western Siberia (Kourovka), Atmos. Meas. Tech., 7, 1763–1776, doi:10.5194/amt-7-1763-2014, 2014.

Berkelhammer, M., Hu, J., Bailey, A., Noone, D. C., Still, C. J., Barnard, H., Gochis, D., Hsiao, G. S., Rahn, T., and Turnipseed, A.: The nocturnal water cycle in an open-canopy forest, J. Geophys. Res.-Atmos., 118, 10225–10242, doi:10.1002/jgrd.50701, 2013.

Chambers, S. D., Wang, F., Williams, A. G., Xiaodong, D., Zhang, H., Lonati, G., Crawford, J., Griffiths, A. D., Ianniello, A., and Allegrini, I.: Quantifying the influences of atmospheric stability on air pollution in Lanzhou, China, using a radon-based stability monitor, Atmos. Environ., 107, 233–243, doi:10.1016/j.atmosenv.2015.02.016, 2015a.

Chambers, S. D., Williams, A. G., Crawford, J., and Griffiths, A. D.: On the use of radon for quantifying the effects of atmospheric stability on urban emissions, Atmos. Chem. Phys., 15, 1175–1190, doi:10.5194/acp-15-1175-2015, 2015b.

Chambers, S. D., Williams, A. G., Crawford, J., and Griffiths, A. D.: On the use of radon for quantifying the effects of atmospheric stability on urban emissions, Atmos. Chem. Phys., 15, 1175–1190, doi:10.5194/acp-15-1175-2015, 2015c.

Craig, H.: Isotopic Variations in Meteoric Waters, Science, 133, 1702–1703, doi:10.1126/science.133.3465.1702, 1961.

Craig, H. and Gordon, L. I.: Deuterium and oxygen-18 variations in the ocean and marine atmosphere, in: Stable isotopes in oceanographic studies and paleotemperatures, Proceedings, Spoleto, Italy, edited by: Tongiogi, E., Pisa, Italy, 9–130, 1965.

Crawford, J., Hughes, C. E., and Parkes, S. D.: Is the isotopic composition of event based precipitation driven by moisture source or synoptic scale weather in the Sydney Basin, Australia?, J. Hydrol., 507, 213–226, doi:10.1016/j.jhydrol.2013.10.031, 2013.

Dansgaard, W.: Stable isotopes in precipitation, Tellus, 16, 436–468, doi:10.1111/j.2153-3490.1964.tb00181.x, 1964.

Decker, M., Pitman, A., and Evans, J.: Diagnosing the seasonal land–atmosphere correspondence over northern Australia: dependence on soil moisture state and correspondence strength definition, Hydrol. Earth Syst. Sci., 19, 3433–3447, doi:10.5194/hess-19-3433-2015, 2015.

Dubbert, M., Cuntz, M., Piayda, A., Maguás, C., and Werner, C.: Partitioning evapotranspiration – Testing the Craig and Gordon model with field measurements of oxygen isotope ratios of evaporative fluxes, J. Hydrol., 496, 142–153, doi:10.1016/j.jhydrol.2013.05.033, 2013.

Evans, J. P. and McCabe, M. F.: Regional climate simulation over Australia's Murray-Darling basin: A multitemporal assessment, J. Geophys. Res.-Atmos., 115, D14114, doi:10.1029/2010JD013816, 2010.

Finnigan, J. J., Clement, R., Malhi, Y., Leuning, R., and Cleugh, H. A.: A Re-Evaluation of Long-Term Flux Measurement Techniques Part I: Averaging and Coordinate Rotation, Bound.-Lay. Meteorol., 107, 1–48, doi:10.1023/A:1021554900225, 2003.

Froehlich, K., Kralik, M., Papesch, W., Rank, D., Scheifinger, H., and Stichler, W.: Deuterium excess in precipitation of Alpine regions – moisture recycling, Isotopes Environ. Health Stud., 44, 61–70, doi:10.1080/10256010801887208, 2008.

Gat, J. R.: Oxygen and hydrogen isotopes in the hydrologic cycle, Annu. Rev. Earth Planet. Sci., 24, 225–262, doi:10.1146/annurev.earth.24.1.225, 1996.

Gat, J. R., Bowser, C. J., and Kendall, C.: The contribution of evaporation from the Great Lakes to the continental atmosphere: estimate based on stable isotope data, Geophys. Res. Lett., 21, 557–560, doi:10.1029/94GL00069, 1994.

Gat, J. R., Klein, B., Kushnir, Y., Roether, W., Wernli, H., Yam, R., and Shemesh, A.: Isotope composition of air moisture over the Mediterranean Sea: an index of the air–sea interaction pattern, Tellus B, 55, 953–965, doi:10.1034/j.1600-0889.2003.00081.x, 2003.

Griffiths, A. D., Parkes, S. D., Chambers, S. D., McCabe, M. F., and Williams, A. G.: Improved mixing height monitoring through a combination of lidar and radon measurements, Atmos. Meas. Tech., 6, 207–218, doi:10.5194/amt-6-207-2013, 2013.

Harding, K. J. and Snyder, P. K.: Modeling the Atmospheric Response to Irrigation in the Great Plains. Part I: General Impacts on Precipitation and the Energy Budget, J. Hydrometeorol., 13, 1667–1686, doi:10.1175/JHM-D-11-098.1, 2012.

He, H. and Smith, R. B.: Stable isotope composition of water vapor in the atmospheric boundary layer above the forests of New England, J. Geophys. Res.-Atmos., 104, 11657–11673, doi:10.1029/1999JD900080, 1999.

Horita, J. and Wesolowski, D. J.: Liquid-vapor fractionation of oxygen and hydrogen isotopes of water from the freezing to the critical temperature, Geochim. Cosmochim. Ac., 58, 3425–3437, doi:10.1016/0016-7037(94)90096-5, 1994.

Huang, L. and Wen, X.: Temporal variations of atmospheric water vapor δD and $\delta^{18}O$ above an arid artificial oasis cropland in the Heihe River Basin, J. Geophys. Res.-Atmos., 119, 11456–11476, doi:10.1002/2014JD021891, 2014.

Hughes, C. E. and Crawford, J.: Spatial and temporal variation in precipitation isotopes in the Sydney Basin, Australia, J. Hydrol., 489, 42–55, doi:10.1016/j.jhydrol.2013.02.036, 2013.

Jana, R. B., Ershadi, A., and McCabe, M. F.: Examining the relationship between intermediate-scale soil moisture and terrestrial evaporation within a semi-arid grassland, Hydrol. Earth Syst. Sci., 20, 3987–4004, doi:10.5194/hess-20-3987-2016, 2016.

Keeling, C. D.: The concentration and isotopic abundances of atmospheric carbon dioxide in rural areas, Geochim. Cosmochim. Ac., 13, 322–334, doi:10.1016/0016-7037(58)90033-4, 1958.

Kurita, N.: Origin of Arctic water vapor during the ice-growth season, Geophys. Res. Lett., 38, L02709, doi:10.1029/2010GL046064, 2011.

Lai, C.-T. and Ehleringer, J.: Deuterium excess reveals diurnal sources of water vapor in forest air, Oecologia, 165, 213–223, doi:10.1007/s00442-010-1721-2, 2011.

Lee, X., Griffis, T. J., Baker, J. M., Billmark, K. A., Kim, K., and Welp, L. R.: Canopy-scale kinetic fractionation of atmospheric carbon dioxide and water vapor isotopes, Global Biogeochem. Cy., 23, GB1002, doi:10.1029/2008GB003331, 2009.

Leuning, R.: The correct form of the Webb, Pearman and Leuning equation for eddy fluxes of trace gases in steady and non-steady state, horizontally homogeneous flows, Bound.-Lay. Meteorol., 123, 263–267, doi:10.1007/s10546-006-9138-5, 2007.

Lin, J. C., Gerbig, C., Wofsy, S. C., Andrews, A. E., Daube, B. C., Davis, K. J., and Grainger, C. A.: A near-field tool for simulating the upstream influence of atmospheric observations: The Stochastic Time-Inverted Lagrangian Transport (STILT) model, J. Geophys. Res., 108, 4493, doi:10.1029/2002JD003161, 2003.

Lu, X., Liang, L. L., Wang, L., Jenerette, G. D., McCabe, M. F., and Grantz, D. A.: Partitioning of evapotranspiration using a stable isotope technique in an arid and high temperature agricultural production system, Agr. Water Manage., 179, 103–109, doi:10.1016/j.agwat.2016.08.012, 2017.

Masson-Delmotte, V., Jouzel, J., Landais, A., Stievenard, M., Johnsen, S. J., White, J. W. C., Werner, M., Sveinbjornsdottir, A., and Fuhrer, K.: GRIP Deuterium Excess Reveals Rapid and Orbital-Scale Changes in Greenland Moisture Origin, Science, 309, 118–121, doi:10.1126/science.1108575, 2005.

Mathieu, R. and Bariac, T.: A numerical model for the simulation of stable isotope profiles in drying soils, J. Geophys. Res.-Atmos., 101, 12685–12696, doi:10.1029/96JD00223, 1996.

McCabe, M. F., Franks, S. W., and Kalma, J. D.: Calibration of a land surface model using multiple data sets, J. Hydrol., 302, 209–222, doi:10.1016/j.jhydrol.2004.07.002, 2005.

McCabe, M. F., Ershadi, A., Jimenez, C., Miralles, D. G., Michel, D., and Wood, E. F.: The GEWEX LandFlux project: evaluation of model evaporation using tower-based and globally gridded forcing data, Geosci. Model Dev., 9, 283–305, doi:10.5194/gmd-9-283-2016, 2016.

Merlivat, L.: Molecular diffusivities of $H_2O^{16}O$, $HD^{16}O$, and $H_2^{18}O$ in gases, J. Chem. Phys., 69, 2864, doi:10.1063/1.436884, 1978.

Merlivat, L. and Jouzel, J.: Global climatic interpretation of the deuterium-oxygen 18 relationship for precipitation, J. Geophys. Res.-Oceans, 84, 5029–5033, doi:10.1029/JC084iC08p05029, 1979.

Noone, D., Risi, C., Bailey, A., Berkelhammer, M., Brown, D. P., Buenning, N., Gregory, S., Nusbaumer, J., Schneider, D., Sykes, J., Vanderwende, B., Wong, J., Meillier, Y., and Wolfe, D.: Determining water sources in the boundary layer from tall tower profiles of water vapor and surface water isotope ratios after a snowstorm in Colorado, Atmos. Chem. Phys., 13, 1607–1623, doi:10.5194/acp-13-1607-2013, 2013.

Pfahl, S. and Wernli, H.: Air parcel trajectory analysis of stable isotopes in water vapor in the eastern Mediterranean, J. Geophys. Res.-Atmos., 113, D20104, doi:10.1029/2008JD009839, 2008.

Pfahl, S. and Wernli, H.: Lagrangian simulations of stable isotopes in water vapor: An evaluation of nonequilibrium fractionation in the Craig-Gordon model, J. Geophys. Res.-Atmos., 114, D20108, doi:10.1029/2009JD012054, 2009.

Risi, C., Noone, D., Frankenberg, C., and Worden, J.: Role of continental recycling in intraseasonal variations of continental moisture as deduced from model simulations and water vapor isotopic measurements, Water Resour. Res., 49, 4136–4156, doi:10.1002/wrcr.20312, 2013.

Samuels-Crow, K. E., Galewsky, J., Sharp, Z. D., and Dennis, K. J.: Deuterium-excess in subtropical free troposphere water vapor: continuous measurements from the Chajnantor Plateau, northern Chile, Geophys. Res. Lett., 41, 8652–8659, doi:10.1002/2014GL062302, 2014.

Simonin, K. A., Link, P., Rempe, D., Miller, S., Oshun, J., Bode, C., Dietrich, W. E., Fung, I., and Dawson, T. E.: Vegetation induced changes in the stable isotope composition of near surface humidity, Ecohydrology, 7, 936–949, doi:10.1002/eco.1420, 2014.

Steen-Larsen, H. C., Johnsen, S. J., Masson-Delmotte, V., Stenni, B., Risi, C., Sodemann, H., Balslev-Clausen, D., Blunier, T., Dahl-Jensen, D., Ellehøj, M. D., Falourd, S., Grindsted, A., Gkinis, V., Jouzel, J., Popp, T., Sheldon, S., Simonsen, S. B., Sjolte, J., Steffensen, J. P., Sperlich, P., Sveinbjörnsdóttir, A. E., Vinther, B. M., and White, J. W. C.: Continuous monitoring of summer surface water vapor isotopic composition above the Greenland Ice Sheet, Atmos. Chem. Phys., 13, 4815–4828, doi:10.5194/acp-13-4815-2013, 2013.

Steen-Larsen, H. C., Sveinbjörnsdottir, A. E., Peters, A. J., Masson-Delmotte, V., Guishard, M. P., Hsiao, G., Jouzel, J., Noone, D., Warren, J. K., and White, J. W. C.: Climatic controls on water vapor deuterium excess in the marine boundary layer of the North Atlantic based on 500 days of in situ, continuous measurements, Atmos. Chem. Phys., 14, 7741–7756, doi:10.5194/acp-14-7741-2014, 2014.

Steen-Larsen, H. C., Sveinbjörnsdottir, A. E., Jonsson, T., Ritter, F., Bonne, J.-L., Masson-Delmotte, V., Sodemann, H., Blunier, T., Dahl-Jensen, D., and Vinther, B. M.: Moisture sources and synoptic to seasonal variability of North Atlantic water vapor isotopic composition, J. Geophys. Res.-Atmos., 120, 5757–5774, doi:10.1002/2015JD023234, 2015.

Tian, L., Masson-Delmotte, V., Stievenard, M., Yao, T., and Jouzel, J.: Tibetan Plateau summer monsoon northward extent revealed by measurements of water stable isotopes, J. Geophys. Res.-Atmos., 106, 28081–28088, doi:10.1029/2001JD900186, 2001.

Uemura, R., Matsui, Y., Yoshimura, K., Motoyama, H., and Yoshida, N.: Evidence of deuterium excess in water vapor as an indicator of ocean surface conditions, J. Geophys. Res.-Atmos., 113, D19114, doi:10.1029/2008JD010209, 2008.

Vallet-Coulomb, C., Gasse, F., and Sonzogni, C.: Seasonal evolution of the isotopic composition of atmospheric water vapour above a tropical lake: Deuterium excess and implication for

water recycling, Geochim. Cosmochim. Ac., 72, 4661–4674, doi:10.1016/j.gca.2008.06.025, 2008.

Wang, L., Niu, S., Good, S. P., Soderberg, K., McCabe, M. F., Sherry, R. A., Luo, Y., Zhou, X., Xia, J., and Caylor, K. K.: The effect of warming on grassland evapotranspiration partitioning using laser-based isotope monitoring techniques, Geochim. Cosmochim. Ac., 111, 28–38, doi:10.1016/j.gca.2012.12.047, 2013a.

Wang, L., Niu, S., Good, S. P., Soderberg, K., McCabe, M. F., Sherry, R. A., Luo, Y., Zhou, X., Xia, J., and Caylor, K. K.: The effect of warming on grassland evapotranspiration partitioning using laser-based isotope monitoring techniques, Geochim. Cosmochim. Ac., 111, 28–38, doi:10.1016/j.gca.2012.12.047, 2013b.

Wei, J., Dirmeyer, P. A., Wisser, D., Bosilovich, M. G., and Mocko, D. M.: Where Does the Irrigation Water Go? An Estimate of the Contribution of Irrigation to Precipitation Using MERRA, J. Hydrometeorol., 14, 275–289, doi:10.1175/JHM-D-12-079.1, 2012.

Welp, L. R., Lee, X., Griffis, T. J., Wen, X.-F., Xiao, W., Li, S., Sun, X., Hu, Z., Val Martin, M., and Huang, J.: A meta-analysis of water vapor deuterium-excess in the midlatitude atmospheric surface layer, Global Biogeochem. Cy., 26, GB3021, doi:10.1029/2011GB004246, 2012.

West, A. G., Patrickson, S. J., and Ehleringer, J. R.: Water extraction times for plant and soil materials used in stable isotope analysis, Rapid Commun. Mass Spectrom., 20, 1317–1321, doi:10.1002/rcm.2456, 2006.

Williams, A. G., Zahorowski, W., Chambers, S., Griffiths, A., Hacker, J. M., Element, A., and Werczynski, S.: The Vertical Distribution of Radon in Clear and Cloudy Daytime Terrestrial Boundary Layers, J. Atmos. Sci., 68, 155–174, doi:10.1175/2010JAS3576.1, 2010.

Williams, A. G., Chambers, S., and Griffiths, A.: Bulk Mixing and Decoupling of the Nocturnal Stable Boundary Layer Characterized Using a Ubiquitous Natural Tracer, Bound.-Lay. Meteorol., 149, 381–402, doi:10.1007/s10546-013-9849-3, 2013.

Xu, X., Werner, M., Butzin, M., and Lohmann, G.: Water isotope variations in the global ocean model MPI-OM, Geosci. Model Dev., 5, 809–818, doi:10.5194/gmd-5-809-2012, 2012.

Zahorowski, W., Chambers, S. D., and Henderson-Sellers, A.: Ground based radon-222 observations and their application to atmospheric studies, J. Environ. Radioact., 76, 3–33, doi:10.1016/j.jenvrad.2004.03.033, 2004.

Zhao, L., Wang, L., Liu, X., Xiao, H., Ruan, Y., and Zhou, M.: The patterns and implications of diurnal variations in the d-excess of plant water, shallow soil water and air moisture, Hydrol. Earth Syst. Sci., 18, 4129–4151, doi:10.5194/hess-18-4129-2014, 2014.